International Journal of Chemical, Materials and Biomolecular Sciences
ISSN: 2415-6620
Vol:10, No:7, 2016

Vibration and Parametric Instability Analysis of Delaminated Composite Beams

A. Szekrényes

***Abstract*—**This paper revisits the free vibration problem of delaminated composite beams. It is shown that during the vibration of composite beams the delaminated parts are subjected to the parametric excitation. This can lead to the dynamic buckling during the motion of the structure. The equation of motion includes time-dependent stiffness and so it leads to a system of Mathieu-Hill differential equations. The free vibration analysis of beams is carried out in the usual way by using beam finite elements. The dynamic buckling problem is investigated locally, and the critical buckling forces are determined by the modified harmonic balance method by using an imposed time function of the motion. The stability diagrams are created, and the numerical predictions are compared to experimental results. The most important findings are the critical amplitudes at which delamination buckling takes place, the stability diagrams representing the instability of the system, and the realistic mode shape prediction in contrast with the unrealistic results of models available in the literature.

***Keywords*—**Delamination, free vibration, parametric excitation, sweep excitation.

I. Introduction

BASICALLY, to calculate the natural frequencies and mode shapes in delaminated beams two approximations are known in the literature: the constrained and free mode models. The constrained mode [1]-[3] means that the deflection of the top and bottom beams of the delaminated region is the same, and consequently this part can be modeled as a single beam having the sum of masses and stiffnesses of the top and bottom beams. In accordance with the free mode model, the top and bottom beams are independent of each other. It was shown that this model leads to significant errors in the free vibration frequencies (e.g. [4]), apart from that the vibration modes involve interpenetration of the top and bottom layers and unrealistically large curvatures. Apparently, the constrained mode model captures better the mechanical problem. The paper by Shen and Grady [5] presented the comparison of the experimentally and numerically determined free vibration frequencies. They also tried to visualize the free vibration mode shapes by making photos on the first vibration mode of delaminated beams. It was shown that the mode shape is asymmetric, i.e. the eigenshape in the first half period is not the reflection image of that in the second one if the delamination is asymmetrically placed between the layers.

Later, numerous papers were published to capture even the delamination opening during the vibration [6], e.g. in [7] nonlinear springs were applied between the top and bottom beams of the delamination. The experimental results presented by Shen and Grady [5] were used, and the asymmetric mode shapes were predicted using the elastic foundation model. In fact, the reason for the delamination opening was still unsolved. The problem of multiple delaminated clamped and clamped-clamped beams was investigated in [8]-[10]. Predictions for the first and second eigenshapes were performed. The literature also presents models based on higher-order analysis [11], [12] and finite elements [13], [14]; however, the basic assumption is that the delamination opening occurs because of the inertia forces. The nonlinear (large amplitude) vibration of delaminated Timoshenko beams was investigated in [15] by considering thermal effects too. An important effect in delaminated beams is the bending-stretching coupling, which was discussed in [16] and it was shown that the simultaneous consideration of the transverse shear effect and longitudinal wave motion improves significantly the accuracy of the model and the agreement with the experimental results.

The main aim of this paper is to show that the delamination opening occurs due to the buckling phenomenon, which is governed by the internal (normal) forces appearing in the delaminated region of the beam. In a previous work, an analytical model based on the system of exact kinematic conditions (SEKC) [17] has been proposed and it has been shown that the delaminated portion is subjected to periodic axial forces [16]. Consequently, if the internal normal force reaches a critical value, the delamination buckles during the vibration. This problem is the special case of parametrically excited systems. This phenomenon takes place in railway wheelsets [18], [19], and among others in machine tools [20]-[22] and milling operations [23]-[25]. In the free vibration of delaminated beams the free vibration frequency and the frequency of parametric excitation is the same. Essentially, the delamination opening is the result of the instability during the vibration of the system.

In this paper, it is shown that parametric excitation exists in the delaminated part if the delamination is embedded. The problem is investigated by the finite element method (FEM). First the basic field equations are presented by using Euler-Bernoulli beam theory. Then, the FE stiffness and mass matrices are constructed based on the potential energy of the system. A transition element is applied in the delamination tips to represent the kinematic continuity between the delaminated and uncracked portions. The dynamic stability of delaminated composite beams is carried out by using the Bolotin's harmonic balance method [26]. The results show

A. Szekrényes is with the Department of Applied Mechanics, Budapest University of Technology and Economics, Budapest, Műegyetem rkp. 5, Building MM, 1111, Hungary (e-mail: szeki@mm.bme.hu).

that the delamination opening is governed by the buckling phenomenon, which takes place if a critical vibration amplitude is exceeded. The present formulation gives some new insights into the dynamic analysis of delaminated beams and it is shown that the structural discontinuities can lead to complex mechanical problems with nonlinear aspects.

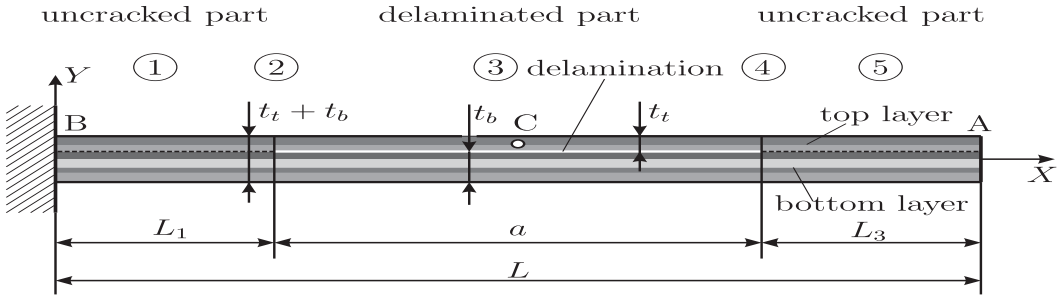

Fig. 1 Layered composite beam with embedded delamination. Notations: (1) - left uncracked portion, (2) - left delamination tip, (3) - delaminated portion, (4) - right delamination tip, (5) - right uncracked portion, A - beam end, B - built-in cross section, C - midpoint in the top beam of region (3)

II. The System of Exact Kinematic Conditions

Let us consider a layered beam with orthotropic plies and an interfacial delamination within the plies as it is shown by Fig. 1. The length of the beam is L, the length of the delamination is a. In Fig. 1, t_t and t_b are the thicknesses of the top and bottom beams. Dividing the uncracked region on the left hand side into two parts in the plane of the delamination and modelling the top and bottom beams as two equivalent single layers (ESL) involves the formulation of kinematic continuity between the top and bottom beams. Fig. 2 (a) shows the vicinity of the left delamination tip of the beam. We know that the in-plane displacement function in Euler-Bernoulli beams can be written as:

$$u_\delta(x,t) = u_\delta^0(x,t) - \frac{\partial v_\delta}{\partial x}(x,t)\, y^{(\delta)}, \tag{1}$$

where $u_{0\delta}$ is the constant part of the in-plane displacement function, v is the transverse deflection and δ can take top or bot (top or bottom beams), respectively (refer to Fig. 2). The kinematic continuity between the top and bottom layers of the uncracked region involves the following condition [17]:

$$u_t\big|_{y^{(t)}=-y_R^t} = u_b\big|_{y^{(b)}=t_b-y_R^b}, \tag{2}$$

where y_R, $y^{(t)}{}_R$, $y^{(b)}{}_R$ are the positions of the global, top and bottom reference planes, respectively. Moreover, in the neutral (reference) plane of the uncracked part the axial displacement is zero, the corresponding condition (depending on the ratio of thicknesses) is:

$$y_R \begin{cases} \le t_b: & u_b\big|_{y^{(b)}=y_R-y_R^b} = 0, \\ \ge t_b: & u_t\big|_{y^{(t)}=-(y_R^t-y_R+t_b)} = 0. \end{cases} \tag{3}$$

Equations (2), (3) are called as the system of exact kinematic conditions (SEKC), which was introduced in [17], [27] for the fracture mechanical analysis of delaminated orthotropic composite plates. Note that if the lay-ups of the whole beam and the top and bottom beams are symmetric or the material is isotropic then $y_R = (t_t + t_b)/2$, $y^t{}_R = t_t/2$, $y^b{}_R = t_b/2$, respectively.

III. Displacement, Strain and Stress Fields in Delaminated Euler-Bernoulli Beams

In this section, the equations of the Euler-Bernoulli beam theory for the laminated beam shown in Fig. 3 (a) is presented. The displacement, strain and stress fields are derived for a further FE discretization. Only orthotropic beams are considered when there is no coupling between the twisting and membrane/bending action of the system.

A. Undelaminated Part

Since the deflections of the uncracked portion ($v_t = v_b = v$) are the same we have the following displacement field (using (1)-(3)):

$$u_t^0 = (y_R^{(t)} - t_b - y_R)\frac{dv}{dx}, u_b^0 = (y_R - y_R^{(b)})\frac{dv}{dx}, \tag{4}$$

$$u_t = (y_R^{(t)} - t_b - y_R)\frac{dv}{dx} - \frac{dv}{dx}y^{(t)}, u_b = (y_R - y_R^{(b)})\frac{dv}{dx} - \frac{dv}{dx}y^{(b)}. \tag{5}$$

The strain and stress fields, moreover the stress resultants (by integrating the stress field) of the top beam become [28]:

$$\begin{aligned} \varepsilon_{xt} &= (y_R^{(t)} - t_b - y_R)\frac{d^2v}{dx^2} - \frac{d^2v}{dx^2}y^{(t)}, \\ \sigma_{xt}^{(k)} &= \bar{C}_{11t}^{(k)}\left((y_R^{(t)} - t_b - y_R)\frac{d^2v}{dx^2} - \frac{d^2v}{dx^2}y^{(t)}\right), \\ N_{xt} &= A_{11t}\left((y_R^{(t)} - t_b - y_R)\frac{d^2v}{dx^2}\right), M_{xt} = -D_{11t}\frac{d^2v}{dx^2}, \end{aligned} \tag{6}$$

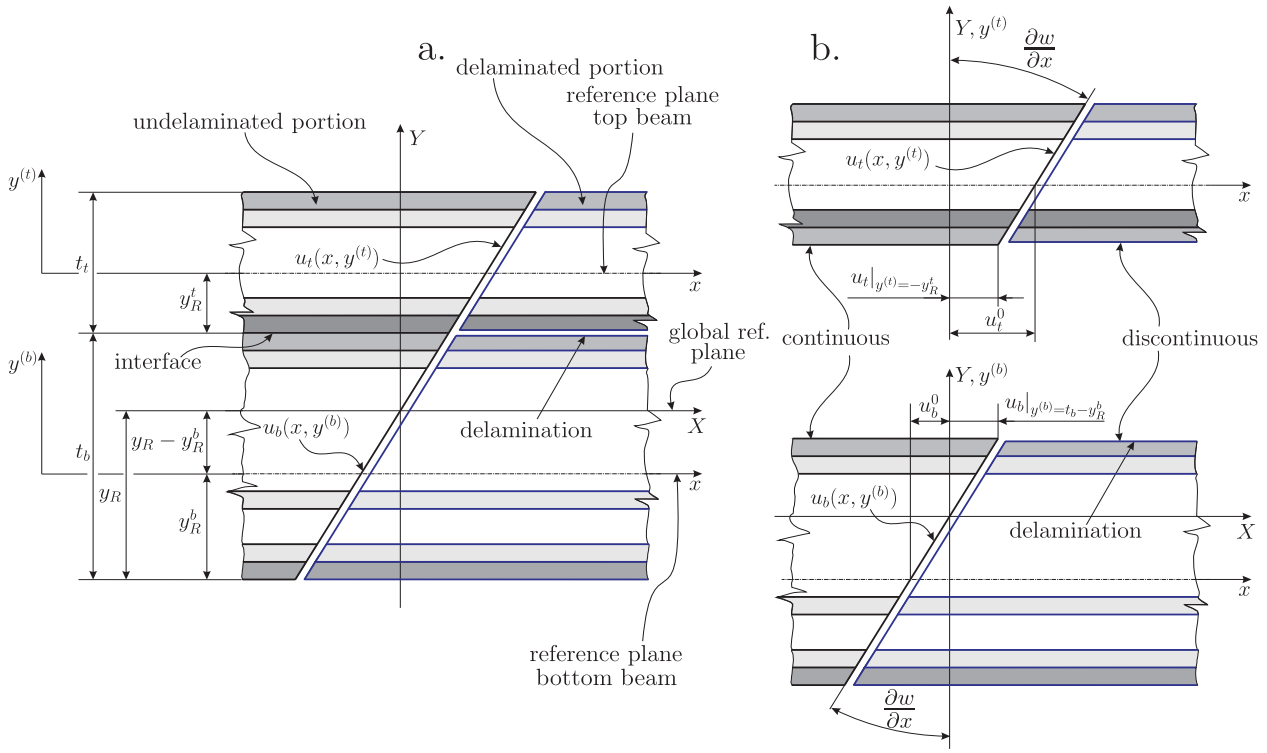

Fig. 2 Formulation of continuity in the uncracked beam portion by using the system of exact kinematic conditions, (a) crack tip region, (b) condition of equal axial displacements at the interface

where $\bar{C}_{11}^{(k)}$ is the corresponding stiffness of the k[th] layer [28]. For a beam-type geometry, it is equal to $E_{11}^{(k)}b$ (modulus of elasticity of the k[th] layer times the width (b)), for plates subjected to cylindrical bending $\bar{C}_{11}^{(k)} = E_{11}^{(k)}b/(1-(\nu_{12}^{(k)})^2)$, where ν_{12} is the Poisson's ratio. For the bottom beam, we obtain the following:

$$\varepsilon_{xb} = (y_R - y_R^{(b)})\frac{d^2v}{dx^2} - \frac{d^2v}{dx^2}y^{(b)},$$
$$\sigma_{xb}^{(k)} = \bar{C}_{11b}^{(k)}\left((y_R - y_R^{(b)})\frac{d^2v}{dx^2} - \frac{d^2v}{dx^2}y^{(b)}\right), \quad (7)$$
$$N_{xb} = A_{11b}(y_R - y_R^{(b)})\frac{d^2v}{dx^2}, M_{xb} = -D_{11b}\frac{d^2v}{dx^2},$$

where A_{11} and D_{11} are the membrane and bending stiffnesses of the top and bottom beams by taking the local neutral planes as reference planes [29]:

$$A_{11} = \sum_{k=1}^{N}\bar{C}_{11}^{(k)}(y_{k+1} - y_k), B_{11} = \frac{1}{2}\sum_{k=1}^{N}\bar{C}_{11}^{(k)}(y_{k+1}^2 - y_k^2),$$
$$D_{11} = \frac{1}{3}\sum_{k=1}^{N}\bar{C}_{11}^{(k)}(y_{k+1}^3 - y_k^3), \quad (8)$$

where B_{11} is the coupling stiffness between the bending and membrane action [28]. For a general lay-up with orthotropic material behavior the neutral plane of the uncracked and delaminated parts can be obtained from the $B_{11} = 0$ condition. Using the stress resultants the potential and kinetic energy of the system can be formulated for the FE discretization.

B. Delaminated Part

For the delaminated part we can simply apply the standard Euler-Bernoulli theory [29], leading to:

$$\varepsilon_{x\delta} = \frac{du_\delta^0}{dx} - \frac{d^2v_\delta}{dx^2}y^{(\delta)}, \sigma_{x\delta}^{(k)} = \bar{C}_{11\delta}^{(k)}\left(\frac{du_\delta^0}{dx} - \frac{d^2v_\delta}{dx^2}y^{(t)}\right), \quad (9)$$
$$N_{x\delta} = A_{11\delta}\frac{du_\delta^0}{dx}, M_{x\delta} = -D_{11\delta}\frac{d^2v}{dx^2}.$$

The FE discretization is carried out in section IV.

IV. Finite Element Discretization

The vibration problem of the delaminated beam shown in Fig. 1 is solved in this paper by using the FEM. The analytical solution based on the SEKC requirements (Fig. 2 (a)) has been presented in a previous work [16] using Timoshenko and Euler-Bernoulli beams. It was shown that the periodic axial forces acting in the delaminated portions involve a system of Mathieu-Hill equations and a complex dynamic stability problem with time dependent stiffness. Fig. 3 (a) shows the stress resultants (M - bending moment, Q - shear force) and

the normal forces (*N*), as well. Fig. 3 (b) shows the five regions in the beam: (1) denotes the uncracked portion in the left hand side, (2) refers to the left transition element, (3) represents the delaminated beam portion with the top and bottom beams, (4) is the right transition element, and finally (5) shows the uncracked part on the right-hand side. Equivalence with notations in Fig. 1 can be established. As it was considered in (1)-(3), the in-plane displacement function is continuous along the uncracked part and discontinuous in the delaminated part. Since the longitudinal wave motion is not independent of the rotation of the cross section, transition elements (2) and (4) are developed to establish the kinematic relationship between the uncracked and delaminated parts, as well as to represent the left and right delamination tips. Finally, in the delaminated portion a regular BEAM2D element [30] is applied with bending, membrane and coupling actions.

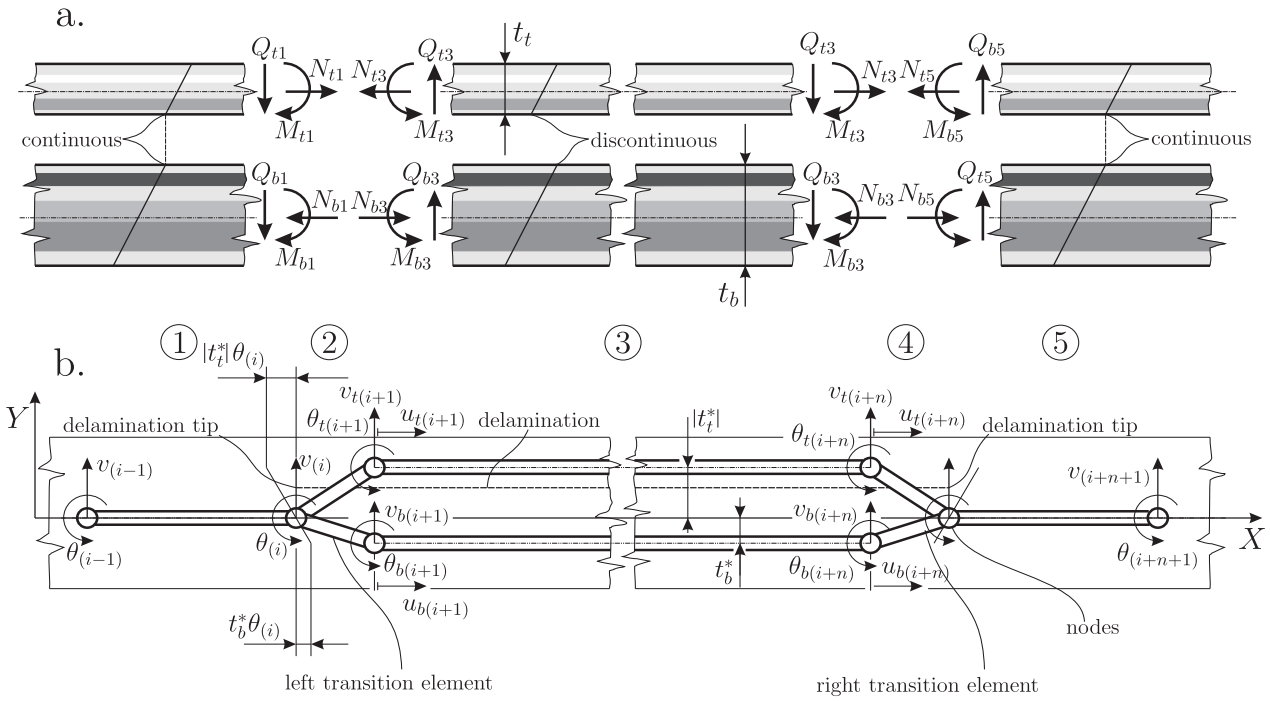

Fig. 3 Stress resultants acting in the transition zones of delaminated layered beams (a). Finite element discretization and nodal DOFs of the layered beam with delamination (b)

The discretization is based on Hamilton's energy principle. The first variation of the total potential energy results in zero [31]:

$$\delta\int_{t_1}^{t_2} I dt = 0, \tag{10}$$

where $I = T - U$ is the Lagrange functional (in the absence of external forces). The strain energy and the kinetic energy for a single element can be formulated through the stress, strain, and displacement fields:

$$U_e = \frac{1}{2}\int_{\Omega_e} \sigma_{ij}\varepsilon_{ij} dV = \frac{1}{2}\mathbf{u}_e^T \mathbf{K}_e \mathbf{u}_e,$$
$$T_e = \frac{1}{2}\int_{\Omega_e} \rho \dot{u}_i \dot{u}_i dV = \frac{1}{2}\dot{\mathbf{u}}_e^T \mathbf{M}_e \dot{\mathbf{u}}_e, \tag{11}$$

where Ω_e is the element domain, ρ is the density, $\mathbf{u}$ is the displacement vector field, $\mathbf{u}_e$ is the vector of nodal displacements, $\mathbf{K}_e$ is the element stiffness matrix, $\mathbf{M}_e$ is the element mass matrix. The total strain end kinetic energy of the system is obtained by summing the element quantities:

$$U = \sum_{N_e} U_e, T = \sum_{N_e} T_e, \tag{12}$$

where, N_e is the number of elements. The assembly of element matrices provides the structural matrices. The application of Hamilton's principle and the assumption of harmonic motion in time results in the equation of motion for the free vibration problem of elastic structures [30]:

$$\mathbf{M}\ddot{\mathbf{U}} + \mathbf{K}\mathbf{U} = \mathbf{0}, \mathbf{U} = \mathbf{A}\cos(\alpha t), \tag{13}$$

where $\mathbf{A}$ is the mode shape vector and α is the free vibration frequency. The FE discretization of the model shown in Fig. 3 involves the development of the matrices for the following regions:

- uncracked parts (1) and (5) in Fig, 3 (b), the stiffness and mass matrices,
- left and right transition elements (2) and (4) in Fig. 3 (b), the stiffness, mass and geometric stiffness matrices,
- delaminated part (3) in Fig. 3 (b), the stiffness, mass and geometric stiffness matrices.

The matrices are presented in [32].

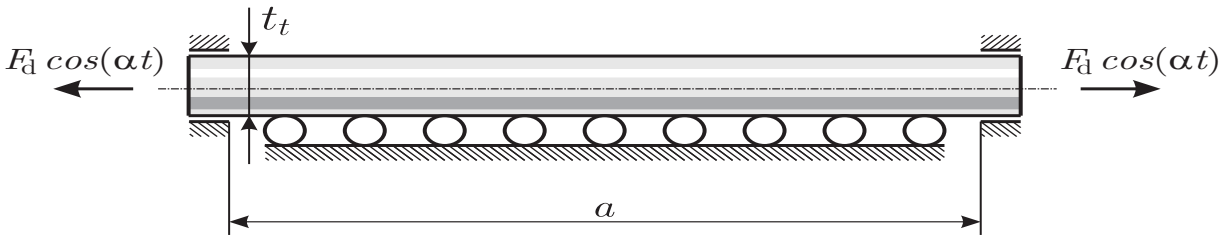

Fig. 4 The top beam of the delaminated region (3) subjected to parametric excitation due to periodic axial force

V. Dynamic Stability Analysis – Parametric Excitation

The delaminated beam portion is loaded by periodic axial forces during the vibration. Therefore, the stiffness of the delaminated part is locally time dependent, however - since the forces are equal in magnitude independently of the lay-up and the location of the delamination [3], [4], [33] - they do not influence the free vibration frequencies and mode shapes at all unless the delamination buckling takes place. The local periodic axial force is the reason for the buckling during the vibration process, and this force induces parametric excitation in the beam as it is shown in Fig. 4. This leads to a dynamic stability problem, which is solved in this section. An important constraint of the problem in Fig. 4 is the sliders allowing the delaminated top beam to buckle only in the upward direction.

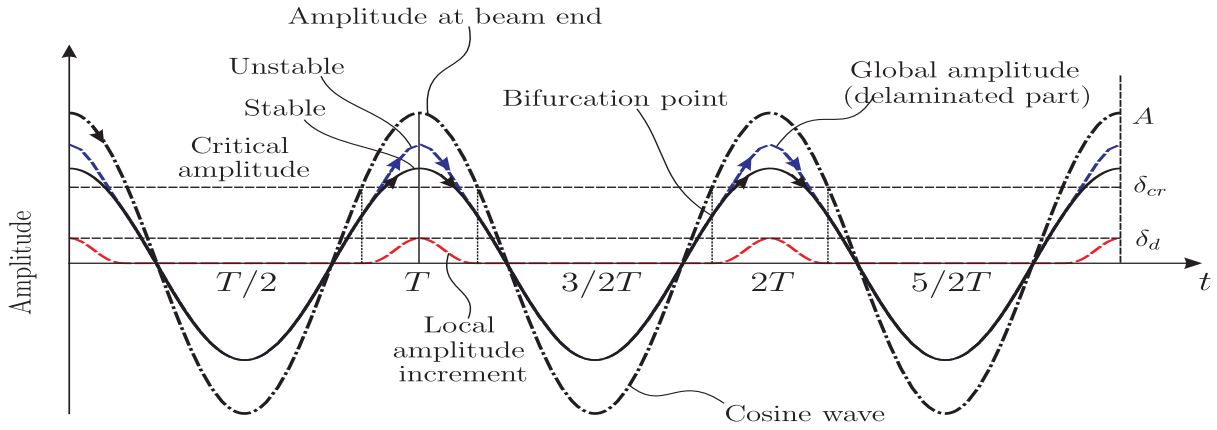

Fig. 5 Time signals of harmonic motion and local amplitude increment in the state of delamination buckling

The equation of motion (system of Mathieu-Hill equations) for parametrically excited discrete systems can be written as [34]–[37]:

$$\mathbf{M}\ddot{\mathbf{U}} + \left(\mathbf{K} + F_d \mathbf{K}_G^0 \cos(\theta t)\right)\mathbf{U} = \mathbf{0}, \tag{14}$$

where **M** and **K** are the structural mass and stiffness matrices, **U** is the structural vector of nodal displacements, F_d is the amplitude of the dynamic force, θ is the frequency of parametric excitation, $\mathbf{K}^0_G$ is the structural geometric stiffness matrix of the system [32]. If the system reaches the critical amplitude during vibration (cross section A in Fig. 1 is considered in this respect), then the top beam of the delaminated part buckles and the time signal of the top delaminated part increases by an incremental amplitude (a small perturbation) as it is shown by Fig. 5. It has already been shown that the normal forces in the top and bottom beams of the delaminated parts are equal to each other [16], and hence the global geometric stiffness during free vibration does not influence the frequencies at all. However, locally the geometric stiffness has to be included for the stability analysis. Assuming an incremental displacement vector in the state of delamination buckling of the top beam the equation of motion modifies to:

$$\mathbf{M}\ddot{\mathbf{U}} + \mathbf{M}_t\ddot{\mathbf{U}}_t + \mathbf{K}\mathbf{U} + \mathbf{K}_t\mathbf{U}_t + \left(F_d \mathbf{K}_{Gt}^0 \cos(\theta t)\right)\mathbf{U}_t = \mathbf{0}, \tag{15}$$

where the matrices with subscript *t* are the mass, stiffness and geometric stiffness matrices of the top beam of the delaminated part. It is very important to note that the matrices are constructed by using a constrained model [32]. Since the system performs harmonic motion in accordance with (13) we have:

$$\mathbf{M}_t\ddot{\mathbf{U}}_t + \mathbf{K}_t\mathbf{U}_t + \left(F_d\mathbf{K}_{Gt}^0\cos(\theta t)\right)\mathbf{U}_t = \mathbf{0}, \tag{16}$$

viz. the stability is carried out only locally on the top beam using clamped-clamped conditions. The increment in the displacement field of the top beam can be written as:

$$\mathbf{U}_t = \mathbf{\Phi}\hat{T}(t), \tag{17}$$

where $\mathbf{U}_t$ is the increment of the amplitude due to delamination buckling, $\mathbf{\Phi}$ is the eigenshape vector of delamination buckling. In accordance with Fig. 5, the following function represents the time dependent part of the local amplitude increment in the top part of the delaminated portion in a kinematically possible way:

$$\hat{T}(t) = \frac{1}{2}\delta_d\left(\cos(\alpha t) - \delta_{cr} + \left|\cos(\alpha t) - \delta_{cr}\right|\right)\left(\delta_{cr} - \cos(\alpha t)\right)^2, \tag{18}$$

where δ_d is the amplitude increment due to delamination buckling, δ_{cr} is the critical amplitude at the end of the beam (at cross section A in Fig. 1), A is the amplitude at the beam end again. The first term in (18) provides a piecewise time signal with positive amplitude increments only (the delamination can buckle only in the upward direction), the second term ensures the kinematically possible motion with zero slopes at the first point of delamination opening and even when the delamination returns and closes. When the delamination buckling appears, the velocity of the points of delaminated beam portion should be equal to the velocity of the global motion at the given point of the beam. Similarly, when the delamination closes, the velocity should be equal to that of the global motion at the given point. This will be shown later in the phase plane portraits. The Fourier series of the time signal given by (18) and Fig. 5 becomes:

$$\begin{aligned}&\hat{T}(t) = a_0 + \sum_{k=1,2,3...}^{\infty} a_k\cos(k\alpha t),\\ &\{a_0, a_k\} = \{a_0(\delta_{cr}), a_k(\delta_{cr})\}, k = 1,2,3,...\end{aligned} \tag{19}$$

that involves odd and even indices equally. If $\delta_{cr} = 0$, then the bifurcation point takes place exactly when the amplitude is zero at every point of the beam. If $\delta_{cr} = A$, then the time signal in (18) vanishes, and no instability occurs. The increment in the vector of nodal displacements becomes:

$$\begin{aligned}&\mathbf{U}_t = \mathbf{a}_0 + \sum_{k=1,2,3...}^{\infty}\mathbf{a}_k\cos(k\alpha t),\\ &\mathbf{a}_0 = a_0\mathbf{\Phi}, \mathbf{a}_k = a_k\mathbf{\Phi}, k = 1,2,3,...\end{aligned} \tag{20}$$

The local vector of nodal accelerations is:

$$\ddot{\mathbf{U}}_t = -\alpha^2\sum_{k=1,2,3...}^{\infty}\mathbf{a}_k k^2\cos(k\alpha t), k = 1,2,3,... \tag{21}$$

Taking these back into (16) and considering the fact that the frequency of free vibration and parametric excitation is the same ($\theta \equiv \alpha$), furthermore applying some trigonometric identities we obtain:

$$\begin{aligned}&\mathbf{K}_t\mathbf{a}_0 + \frac{1}{2}F_d\mathbf{K}_{Gt}^0\mathbf{a}_1 = \mathbf{0}\\ &(\mathbf{K}_t - \alpha^2\mathbf{M}_t)\mathbf{a}_1 + \frac{1}{2}F_d\mathbf{K}_{Gt}^0(2\mathbf{a}_0 + \mathbf{a}_2) = \mathbf{0}\\ &(\mathbf{K}_t - k^2\alpha^2\mathbf{M}_t)\mathbf{a}_k + \frac{1}{2}F_d\mathbf{K}_{Gt}^0(\mathbf{a}_{k-1} + \mathbf{a}_{k+1}) = \mathbf{0}, k = 2,3,...\end{aligned} \tag{22}$$

where F_d is the dynamic force amplitude. The equations in matrix form can be given as:

$$\begin{pmatrix} \mathbf{K}_t & \frac{1}{2}F_d\mathbf{K}_{Gt}^0 & 0 & 0 & \cdots\\ F_d\mathbf{K}_{Gt}^0 & \mathbf{K}_t - \alpha^2\mathbf{M}_t & \frac{1}{2}F_d\mathbf{K}_{Gt}^0 & 0 & \cdots\\ 0 & \frac{1}{2}F_d\mathbf{K}_{Gt}^0 & \mathbf{K}_t - 4\alpha^2\mathbf{M}_t & \frac{1}{2}F_d\mathbf{K}_{Gt}^0 & \cdots\\ 0 & 0 & \frac{1}{2}F_d\mathbf{K}_{Gt}^0 & \mathbf{K}_t - 9\alpha^2\mathbf{M}_t & \cdots\\ \vdots & \vdots & \vdots & \vdots & \ddots \end{pmatrix}\begin{pmatrix}\mathbf{a}_0\\ \mathbf{a}_1\\ \mathbf{a}_2\\ \mathbf{a}_3\\ \vdots\end{pmatrix} = \begin{pmatrix}\mathbf{0}\\ \mathbf{0}\\ \mathbf{0}\\ \mathbf{0}\\ \vdots\end{pmatrix}. \tag{23}$$

This method is called the harmonic balance [26], and it was applied to delaminated composite beams in [32]. The critical value of the force amplitude, F_d can be obtained by setting the determinant of the matrix in (23) to be equal to zero and by taking back any of the free vibration frequencies determined by (13). Based on the critical force and the normal force arising during vibration with an actual amplitude the critical amplitude of free vibration at cross section A in Fig. 1 - at which delamination buckling takes place - can be obtained. The buckled shape of the top beam can be obtained from any of (22) (infinite number of solutions). However, there is a very little difference among the eigenshapes from (22) and the first eigenshape of static stability calculated by:

$$(\mathbf{K}_t + \lambda\mathbf{K}_{Gt})\mathbf{U}_t = \mathbf{0}, \tag{24}$$

where λ is the eigenvalue giving the critical force under static buckling of the top beam in the delaminated part with clamped-clamped conditions, $\mathbf{K}_{Gt}$ is the geometric stiffness of the top beam in the delaminated part. The amplitude increment (δ_d, see Fig. 5) due to buckling is determined by a condition of constant arc length of the top beam during the vibration (see later).

VI. Experiments

The experiments on unidirectional glass-polyester specimens with embedded delaminations have been carried

out in a recent paper [16]. The main properties of the tested beams were: E_{11} = 33 GPa, ρ=1330 kg/m^3, L = 180 mm, b = 20 mm. The total thickness of the beams was always $t_t + t_b$=6.2 mm. Four different delamination lengths were applied: a=60, 80, 100 and 120 mm. More geometric data are provided in Table I, refer to Fig. 1, as well. The delamination was a thin polyamid insert which was placed between the layers during the manufacturing process. The total number of layers was 14. On the other hand, the through-thickness position of the delaminations was also varied. In this respect, four different variants were used: interface 0 means that the delamination lies in the midplane of the beams, interface 2 refers to the fact that the top and bottom beams of the delaminated part consists of two sub-beams with 5 and 9 layers. Consequently, interface 4 and interface 6 mean that the division of the delaminated parts involves 3 and 11, and 1 and 13 layers, respectively. In the sequel the beams are referred to by using the crack length/interface code, i.e. 60/6 means the beam with crack length of 60 mm and with a delamination at interface 6. The natural frequencies have been determined by modal hammer and sweep excitation tests [16].

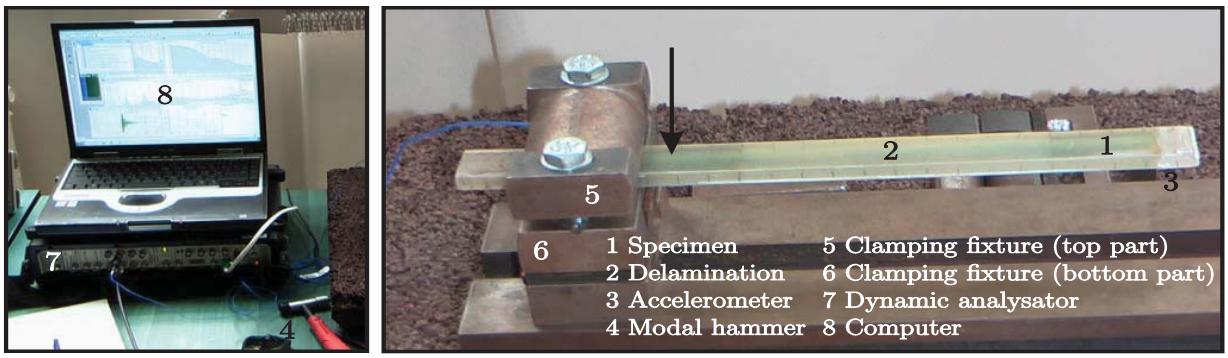

Fig. 6 Experimental setup for frequency and mode shape measurement by modal hammer test

A. Modal Hammer Test

In this test, the delaminated beams were rigidly fixed at one end by using a clamping fixture in accordance with Fig. 6. An accelerometer with very small mass (0.2 g) was attached close to the free end. A modal hammer with steel head was applied and the beam was hit by the hammer close to the built-in end of the beam. The cables of the accelerometer and the hammer were plugged into a Brüel and Kjaer dynamic analyser and the measured signals were processed by a notebook. The maximum of the impact force was between 55 and 85 N in each case. The frequencies were determined from the peaks of the frequency response functions [38].

TABLE I
GEOMETRY OF THE TESTED DELAMINATED COMPOSITE BEAMS

a [mm]	60	80	100	120
L_1 [mm]	58	46	33	24
L_3 [mm]	62	54	47	36

B. Sweep Excitation Test

During the sweep excitation test the configuration was almost the same as that detailed in the former subsection. However, in this case the clamping fixture was bolted to the vibro-head of the exciter. A magnetic accelerometer was placed onto the clamping fixture, while the small accelerometer was attached to the beam end. The accelerations in the assigned points were measured with respect to each other, simultaneously a force excitation was generated through the vibro-head of the exciter. The system generated the excitation in the frequency interval of 0 Hz - 6 kHz during 30 seconds. The sweep excitation signal was provided by a generator with constant force amplitude, and the generator was connected to an amplifier and then to the exciter, respectively.

The displacement amplitude at the beam end (cross section A in Fig. 1) was measured based on the accelerations and was between 0.5 and 0.65 mm in the first frequency; however, it decreased subsequently in higher modes because of the constant amplitude force excitation. Finally, the natural frequencies were read from the generated frequency response functions.

VII. RESULTS AND DISCUSSION

A. Free Vibration Frequencies

In [16] analytical models based on Euler-Bernoulli and Timoshenko beam theories have been presented. In this paper we summarize the results and make a comparison to those calculated by the FE model. The measured frequency response functions determined by modal hammer and sweep excitation tests are shown in Figs. 7 (a) and 8 for certain beam configurations. The first four frequencies were identified by the peak points in the graphs. The mode shape is also shown in Fig. 7 (b) by color distribution. Tables II and III present the results for the 60/0, 60/2, 60/4 and 60/6 composite beams. It is seen that the agreement between the modal hammer test and sweep excitation results is quite good. Considering the analytical models, the agreement with the experiments is better if the longitudinal wave is not considered. In the FE model, 7 elements were applied along the uncracked and delaminated portions for the beams with 60 and 80 mm long delaminations, 8 elements were applied at each region for the beams with 100 and 120 mm long delaminations. The convergence of the frequencies was checked and it was found

that by further increasing the number of elements the results changed with less than 1 percent. The length of the transition elements was 1 mm, no significant effect of the transition element length on the frequencies was found. The FE model gives almost exactly the same result as the corresponding analytical model (E.-B. with longitudinal vibration) for each frequency. The analytical and FE models overestimate the first frequency measured from modal hammer test by 23%, the second one by 31%, the third one by 17% and the fourth one by 21% for the 60/0 beam. The results of the sweep excitation test (60/0 beam) are closer to the model predictions, especially the first frequency, where the difference is 7%. For the second, third and fourth frequencies 23, 13 and 21% differences were experienced. The results for the other beam configurations are documented in [16], [32]. It has to be highlighted that better agreement can be achieved between the experimental and analytical/numerical results for the second, third and fourth frequencies by considering the transverse shear effect [16]. It is shown in the former paper, that transverse shear does not affect fundamentally the first vibration frequency. The possible damping effect [38], [39] was also investigated and was found to influence the frequencies with less than 1% [40].

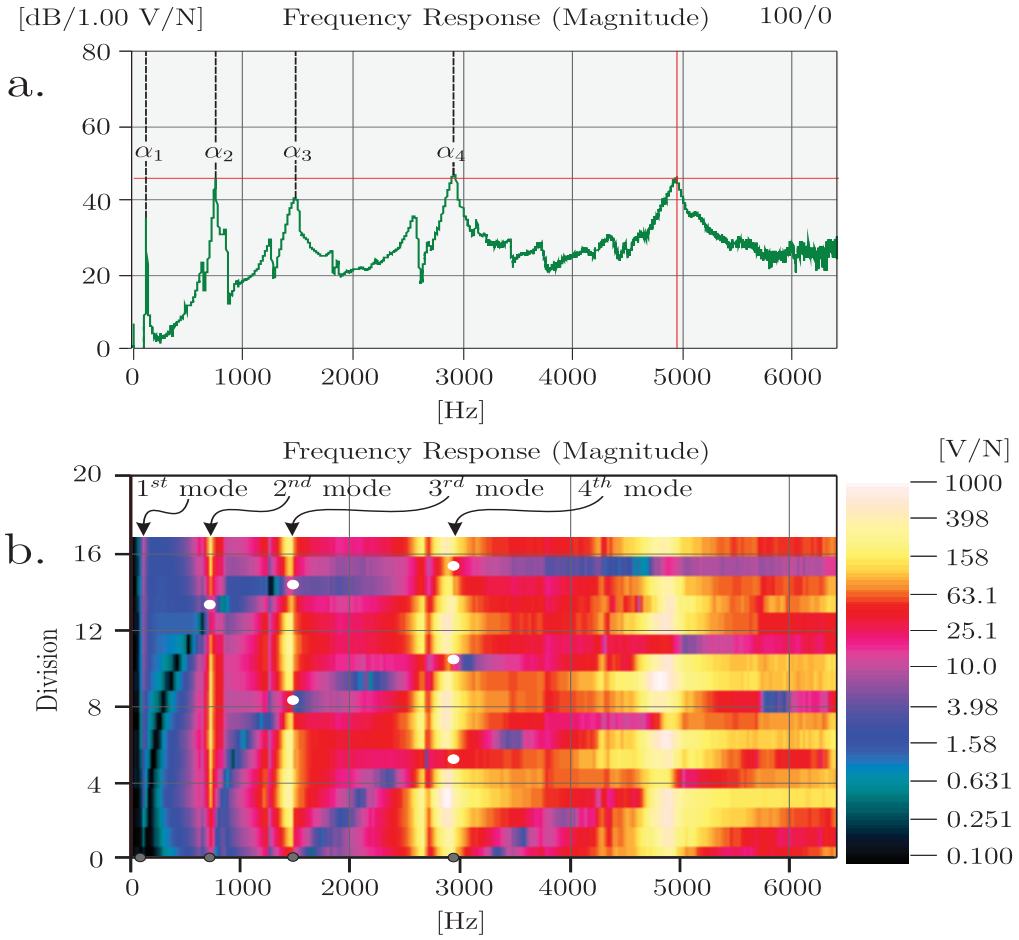

Fig. 7 Frequency response (a) and mode shape distribution by color scale (b) by modal hammer test for the 100/0 composite beam

B. Periodic Normal Forces

The distribution of the normal forces in the delaminated beam portions are shown in Figs. 9 and 10 for the 80/6 and 120/6 beams when the vibration amplitude is 1 mm at the end of the beams. The normal forces were calculated using (6), (7) and (9). It can be seen that the finite element and analytical results are basically the same. An important result is that the normal forces are always equal in magnitude for the top and bottom beams independently of the location of the delamination in the through-thickness direction. This aspect - which holds even when the lay-up of the whole, top and bottom beams is asymmetric - has already been shown in the literature [3], [4] based on geometrical and equilibrium considerations. For the first and second free vibration modes (Figs. 9 (a) and (b); 10 (a) and 10 (b)) the normal forces have constant distributions in the delaminated parts. On the contrary, for the third and fourth vibration modes the forces change exponentially. These periodic forces change the bending stiffness of the delaminated portion, and so the stiffness becomes time dependent. However, since the forces are always equal to each other in magnitude, globally there is no effect of the parametric excitation on the free vibration

frequencies; in other words, they eliminate the effect of each other at every time moment. However, if the amplitude reaches a critical value, then the delamination buckling can take place. It will be shown later, that during small-amplitude vibration this occurs only if the top beam is very thin.

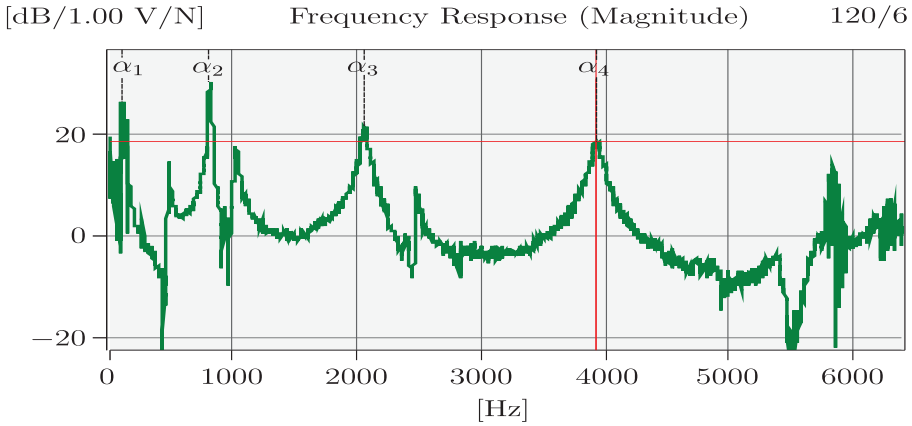

Fig. 8 Frequency response by sweep excitation test for the 120/6 composite beam

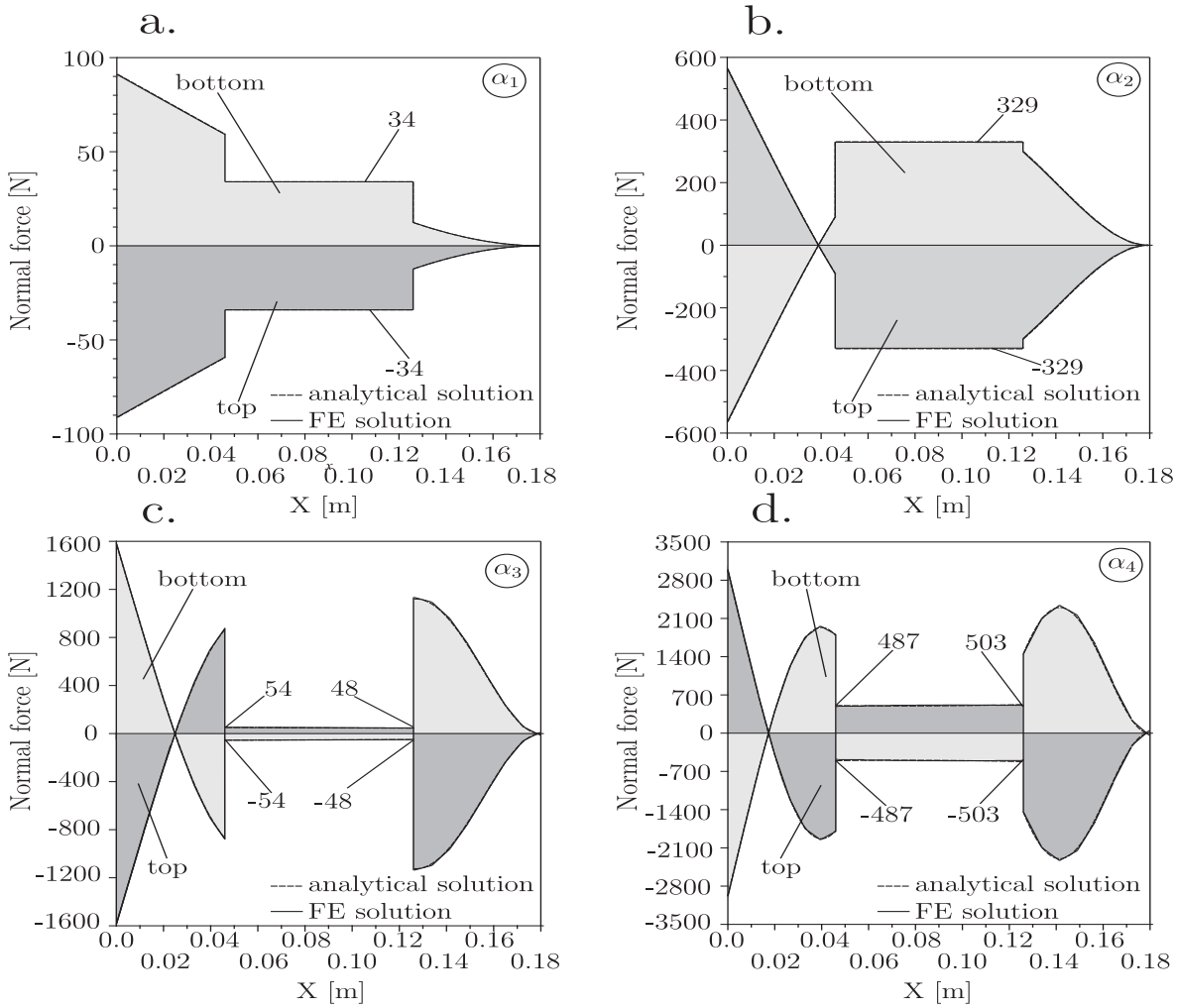

Fig. 9 Distribution of the normal force along the top and bottom beam axes in the case of the first four free vibration frequencies of the 80/6 beam

TABLE II
FREE VIBRATION FREQUENCIES FOR THE (60/0) AND (60/2) COMPOSITE BEAMS IN [HZ]

Beam configuration	60/0				60/0			
	Free vibration frequencies [Hz]				Free vibration frequencies [Hz]			
Method, theory	α_1	α_2	α_3	α_4	α_1	α_2	α_3	α_4
Modal hammer test	124	731	1737	3765	105	781	1706	3642
Sweep excitation test	142	780	1798	3776	138	790	1830	3780
E.-B.	123	659	2013	4345	128	689	2112	4469
E.-B. with longitudinal vibration	152	961	2025	4566	153	965	2153	4749
E.-B. with long. (FEM)	152	960	2025	4567	153	965	2160	4756

Note:
- E.-B. - analytical solution based on Euler-Bernoulli beam theory considering transverse vibration only
- E.-B. with longitudinal vibration - analytical solution based on Euler-Bernoulli beam theory considering transverse and longitudinal vibration
- E.-B. with long. (FEM) - finite element solution based on Euler-Bernoulli beam theory considering transverse and longitudinal vibration

TABLE III
FREE VIBRATION FREQUENCIES FOR THE (60/4) AND (60/6) COMPOSITE BEAMS IN [HZ]

Beam configuration	60/4				60/6			
	Free vibration frequencies [Hz]				Free vibration frequencies [Hz]			
Method, theory	α_1	α_2	α_3	α_4	α_1	α_2	α_3	α_4
Modal hammer test	112	712	1891	3854	126	738	2124	4196
Sweep excitation test	136	732	1948	3940	138	718	2112	4232
E.-B.	138	765	2328	4730	148	863	2541	5011
E.-B. With longitudinal vibration	153	959	2389	5000	153	963	2610	5203
E.-B. with long. (FEM)	152	961	2400	5007	154	966	2625	5224

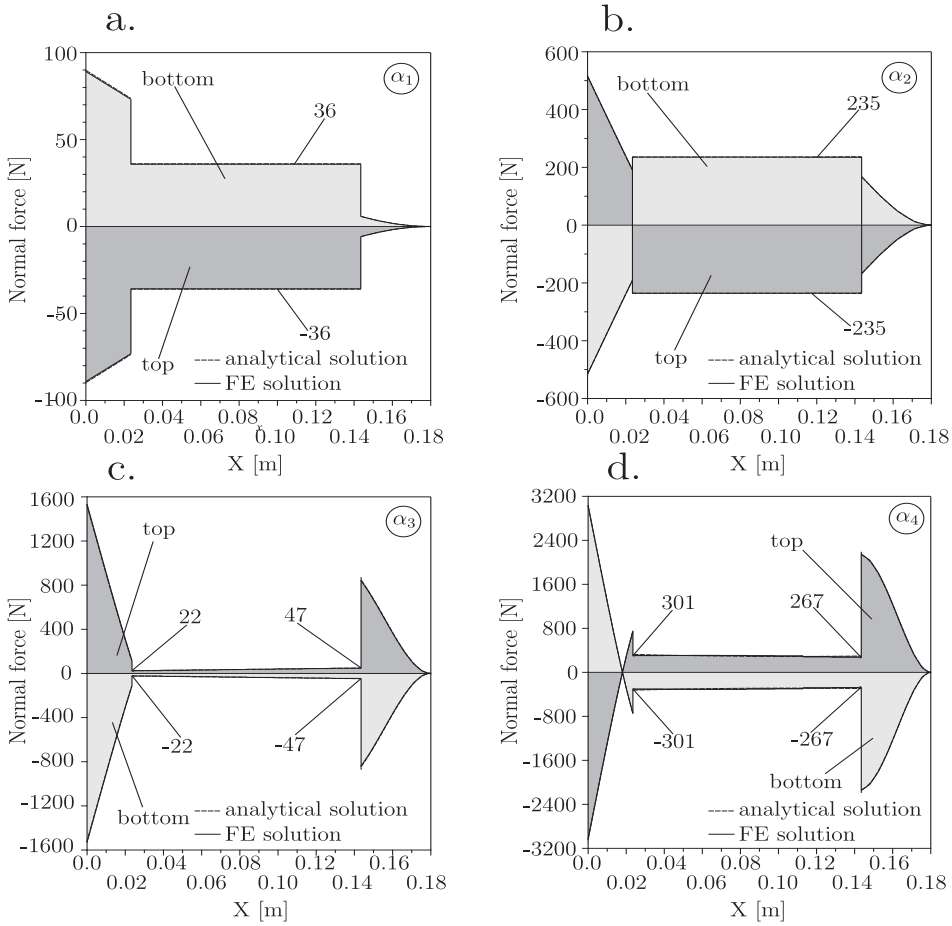

Fig. 10 Distribution of the normal force along the top and bottom beam axes in the case of the first four free vibration frequencies of the 120/6 beam

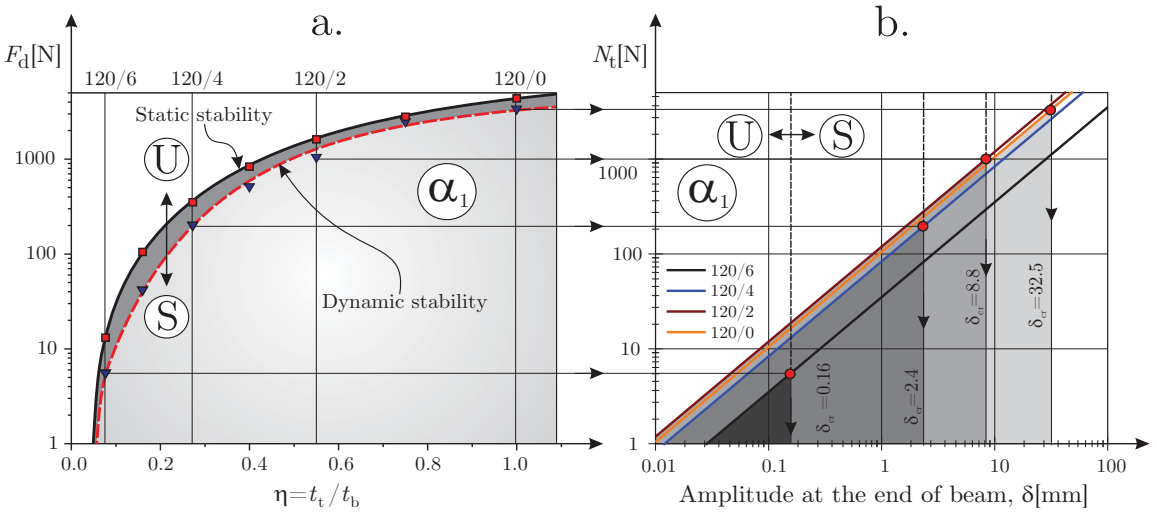

Fig. 11 Stability diagram of the composite beam with a=120 mm long delamination for the 1st free vibration frequency: (a) critical values of the normal force under static and dynamic stability, (b) determination of the critical vibration amplitudes. Note: the vertical axes apply logarithmic scales

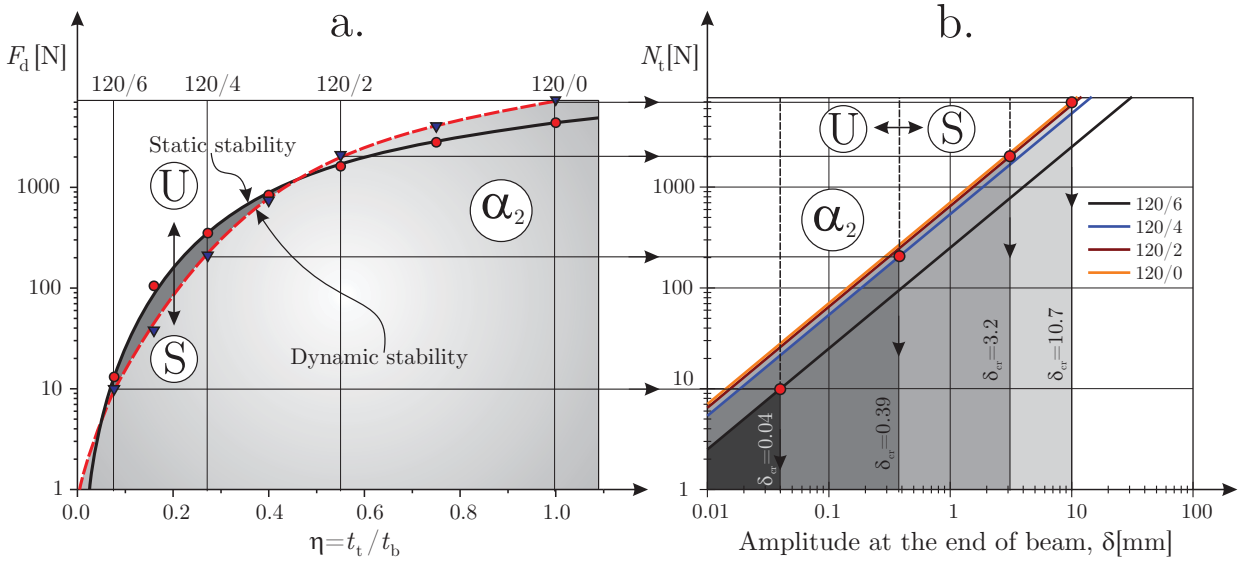

Fig. 12 Stability diagram of the composite beam with *a*=120 mm long delamination for the 2nd free vibration frequency: (a) critical values of the normal force under static and dynamic stability, (b) determination of the critical vibration amplitudes. Note: the vertical axes apply logarithmic scales

C. Dynamic Stability Analysis

The dynamic stability analysis of the beam configurations was carried out based on Section V. The critical forces for the beams at each frequency were determined by setting the determinant of the coefficient matrix in (23) to zero. The distribution of the normal force along the uncracked region was considered in the construction of the $\mathbf{K}^0_{Gt}$ geometric stiffness in (23). Since the normal force is not constant in the case of the third and fourth frequencies, the critical force means the value of the force at the right delamination tip. In each case the order of the determinant was increased until a reasonable convergence of the force was achieved (a 5% criterion against the forces obtained by two subsequent determinants was applied). In general, 9th - 14th order determinants provided the required convergence. Figs. 11-14 present the stability diagrams of the beams with 120 mm long delamination for the first to the fourth free vibration frequencies. In Figs. 11 (a), 12 (a), 13 (a) and 14 (a) the stability limits are shown, for the sake of completeness even the limits under static stability (by (24)) are given. Each figure was constructed using logarithmic scale on the vertical axis. It is important to see that the dynamic stability limit is somewhat less than the static one in most of the cases. The critical amplitudes at the beam end can be calculated using Figs. 7 (b), 8 (b), 9 (b) and 10 (b). Reaching the critical amplitude means that the top beam buckles during the vibration, and local

stability loss takes place. Plotting the normal force-beam end amplitude relationship (linear relation using a logarithmic horizontal scale) and finding the intersection points by projecting the points of Figs. 11 (a), 12 (a), 13 (a) and 14 (a) results in the critical amplitudes. For the second, third and fourth frequencies the stability diagrams are shown in Figs. 12-14. Based on the critical amplitudes calculated, it is concluded that the system is the most unstable under the fourth frequency, then under the second one. It is followed by the first one, and the third one is the most stable (the highest critical amplitudes are required for delamination buckling in this latter case). For the other beam configurations the critical forces and amplitudes are documented in [32]. The main conclusions and the order of frequencies from the point of view of instability are essentially the same. Note that in each case the absolute value of the critical displacement is presented.

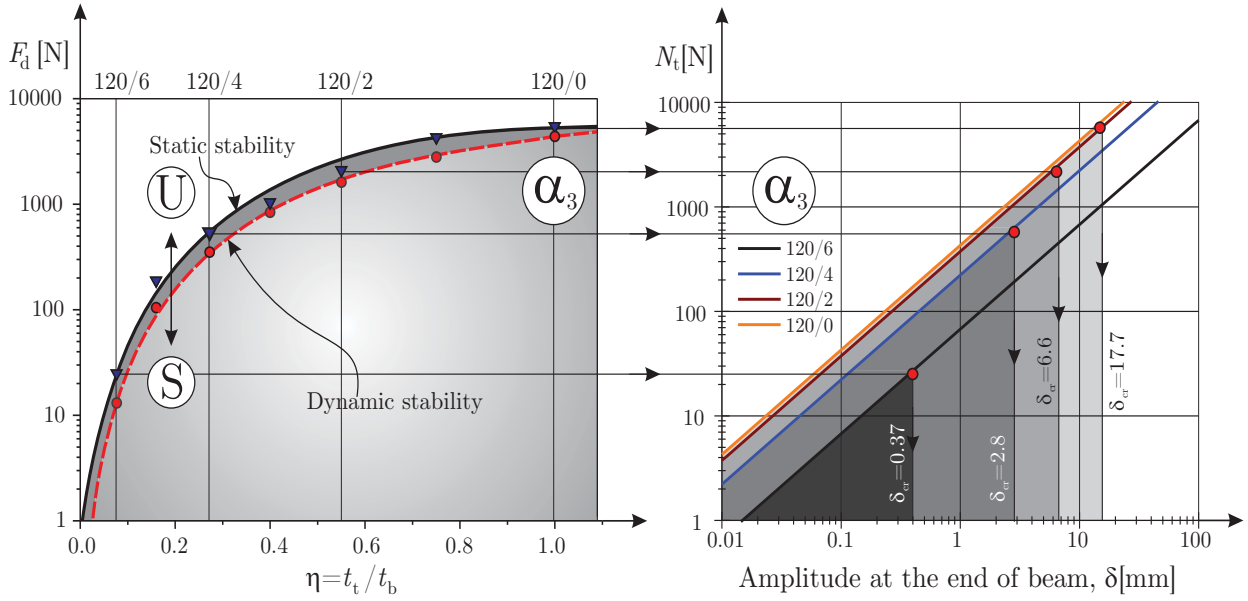

Fig. 13 Stability diagram of the composite beam with a=120 mm long delamination for the 3rd free vibration frequency: (a) critical values of the normal force under static and dynamic stability, (b) determination of the critical vibration amplitudes. Note: the vertical axes apply logarithmic scales

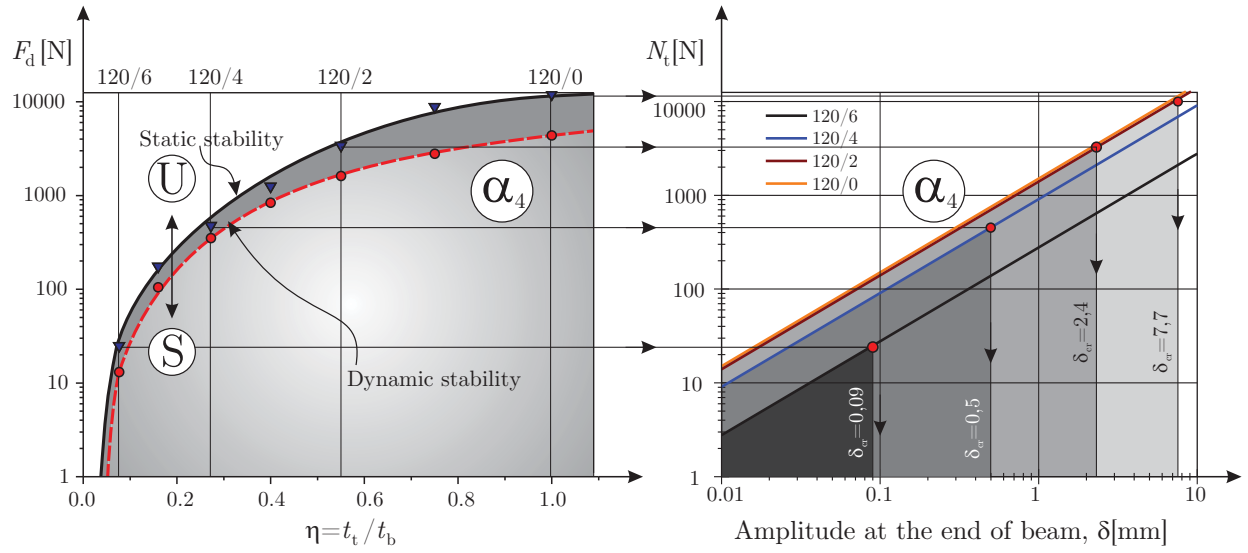

Fig. 14 Stability diagram of the composite beam with a=120 mm long delamination for the 4th free vibration frequency: (a) critical values of the normal force under static and dynamic stability, (b) determination of the critical vibration amplitudes. Note: the vertical axes apply logarithmic scales

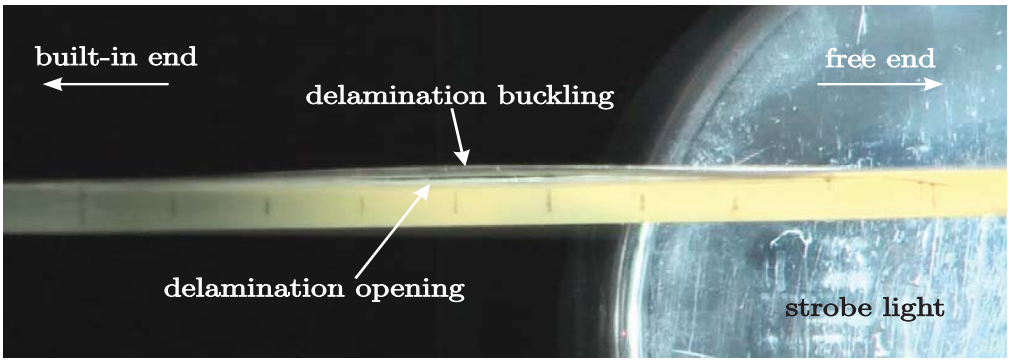

Fig. 15 Delamination buckling and opening during vibration of the 80/6 beam with excitation frequency of 128 Hz (1st natural frequency), beam end amplitude of 0.98 mm, strobe light frequency of 43 Hz

Fig. 15 shows the state of delamination buckling of the 80/6 beam in the case of the first natural frequency if the amplitude at the free end (cross section A in Fig. 1) is 0.98 mm and the excitation frequency is 128 Hz. The system was subjected to a strobe light applying one third of the excitation frequency. It can be seen how the delamination opens and buckles as the beam moves in the upward direction. It is very important to note that during the observation of the first eigenshape the motion was found to be absolutely impact-free and the closure of the delamination was a smooth transition.

D.Mode Shapes with Delamination Buckling

If the system vibrates below the stability limit (critical amplitude) then it is governed by the model developed in section IV. However, if the stability limit is exceeded, then the delamination buckling takes place and the developed model is no longer valid from the mechanical point of view. The system becomes nonlinear and the principle of superposition is no longer applicable. Nevertheless, considering small amplitude vibration (1.5 - 3 mm amplitude at beam end) it is seen that the delamination buckles only for the .../6 configurations. In the case of the 120/6 beam, the mass of the top beam is less than 5% of the total mass of the beam, moreover it contributes with a negligible value to the bending stiffness of the beam. Under these circumstances, the prediction of the mode shapes under stability loss is possible by superimposing the free vibration mode shape and the buckled shape, respectively. In other words, we neglect the interaction of delamination buckling and free vibration. The amplitude of the relative buckled eigenshape was controlled by the arc length of the beam. More exactly, the arc length of the local buckling eigenshape minus the relative axial displacement of the delamination tips was equated to the delamination length at the end of the half period (when the highest amplitude is reached) with two decimals accuracy.

Figs. 16 and 17 present the mode shape predictions for the 80/6 and 120/6 beams. The first four free vibration frequencies are considered; in each case the critical amplitude is indicated in the figures. The first free vibration mode shape has already been predicted in numerous papers (e.g.: [5]), the second one has been predicted in [33]; however, no approximations have been presented for the higher vibration modes. This is important, because the system response under excited vibration is the superposition of the free vibration eigenshapes. The highest relative buckling amplitude is obtained in the case of the second natural frequency. On the contrary, under the third frequency, the former value is very small. It can be seen that the amplitude of instability is negative for the third and fourth vibration frequencies. Unfortunately, it was not possible to observe the higher eigenshapes experimentally, only the first one. The reason for that is the experimental equipment is based on force excitation, the force is proportional to the square of the frequency.

To reach a reasonable vibration amplitude at the free end (1-2 mm) under higher vibration modes significantly higher forces are required than in the case of the first mode. In spite of that, it can be assumed that the mode shapes presented in Figs. 16 and 17 are close to the reality in these particular cases. It is also clear that the nonlinear analysis is required as a next step.

E. Phase Plane Portraits

Based on the linear prediction of the mode shapes with local stability loss the phase plane portraits for the midpoint of the top beam in the delaminated part (point C in Fig. 1) are plotted in Figs. 18 and 19. Under harmonic motion, the phase plane portraits are in fact simple ellipses. However, if the delamination buckles then the amplitude and more importantly the velocity of the points change significantly. It has to be mentioned that when the critical amplitude is reached then at the moment of delamination opening and closing the velocity of the delamination midpoint must be the same as the corresponding point in the bottom beam (kinematic condition). This condition is ensured by the time signal of (18). Depending on the bending vibration mode, the phase plane portraits show some special trajectories. For instance, for the 80/6 beam - depending on the vibration amplitude at the beam end - the first natural frequency involves “guitar body” and “icecream in cone” shape trajectories, respectively (Fig. 18 (a)). In accordance with Fig. 18 (b) the “carpet-beater” trajectory is typically related to the second free vibration frequency. For the third and fourth frequencies the associated shapes are “pac man”, “pincers”, and “croissant”, respectively. The phase plane trajectories of the 120/6 beam are presented

in Fig. 19. The midpoint of delamination provides "light bulb" shape trajectories for the first frequency, otherwise the higher vibration modes involve similar shapes to those given by Figs. 18 (b)-(d). The overall conclusion related to Figs. 18 and 19 are that there are significant changes in the trajectories of the points of the top beam undergoing delamination buckling. This aspect of the problem was also detailed in [41] for delaminated plates.

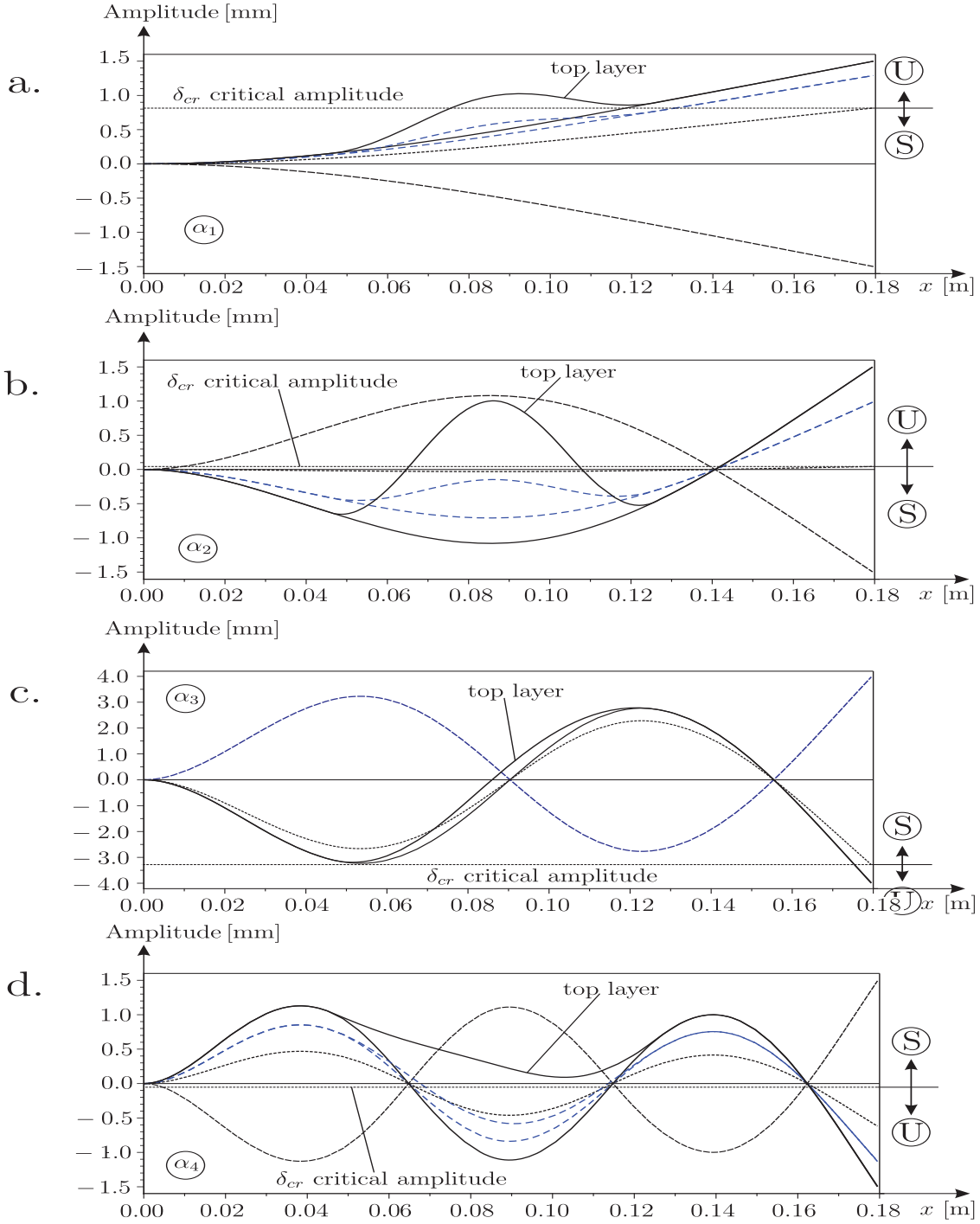

Fig. 16 Mode shape prediction for the 80/6 beam for the first four free vibration frequency with delamination buckling

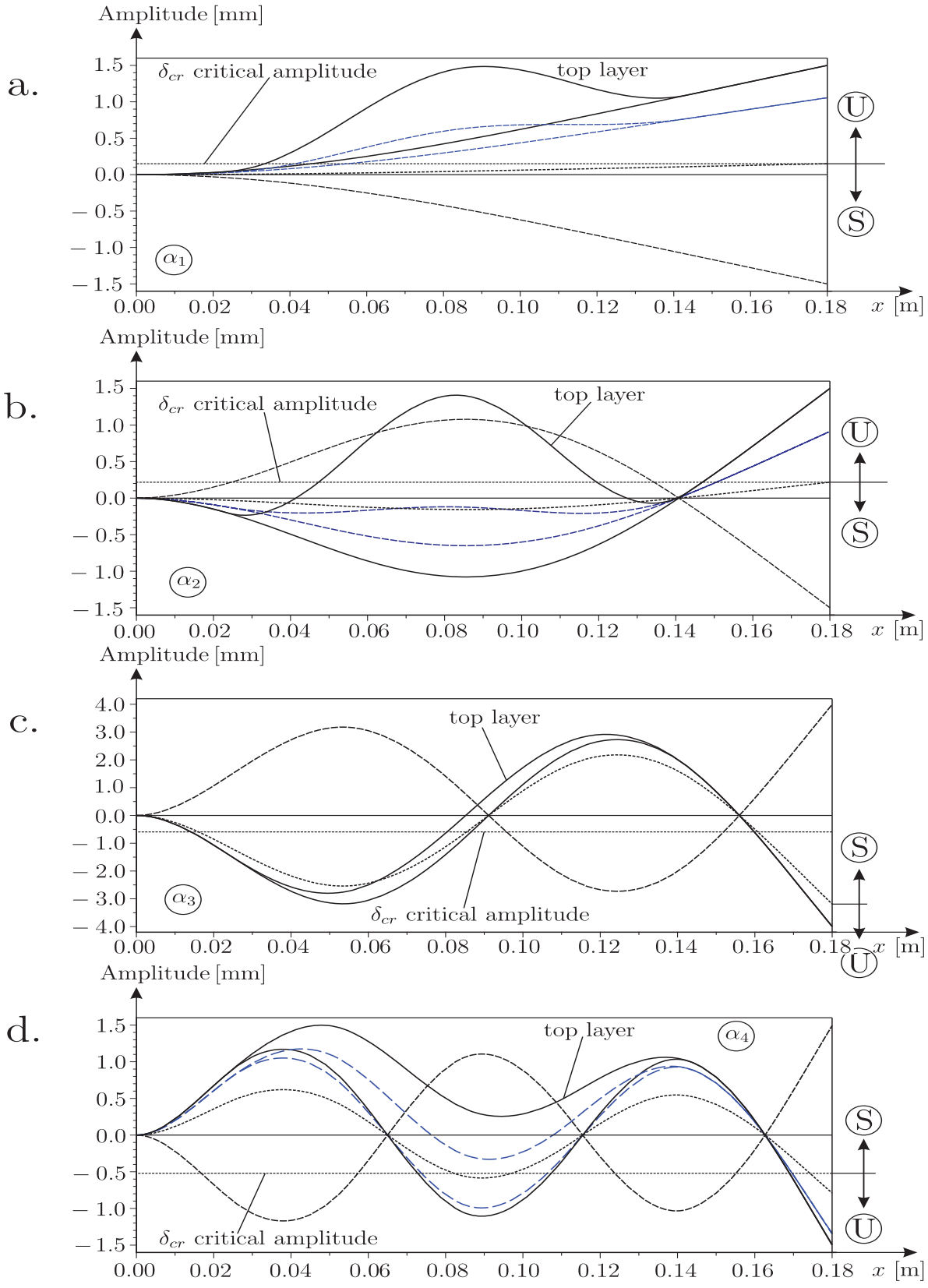

Fig. 17 Mode shape prediction for the 120/6 beam for the first four free vibration frequency with delamination buckling

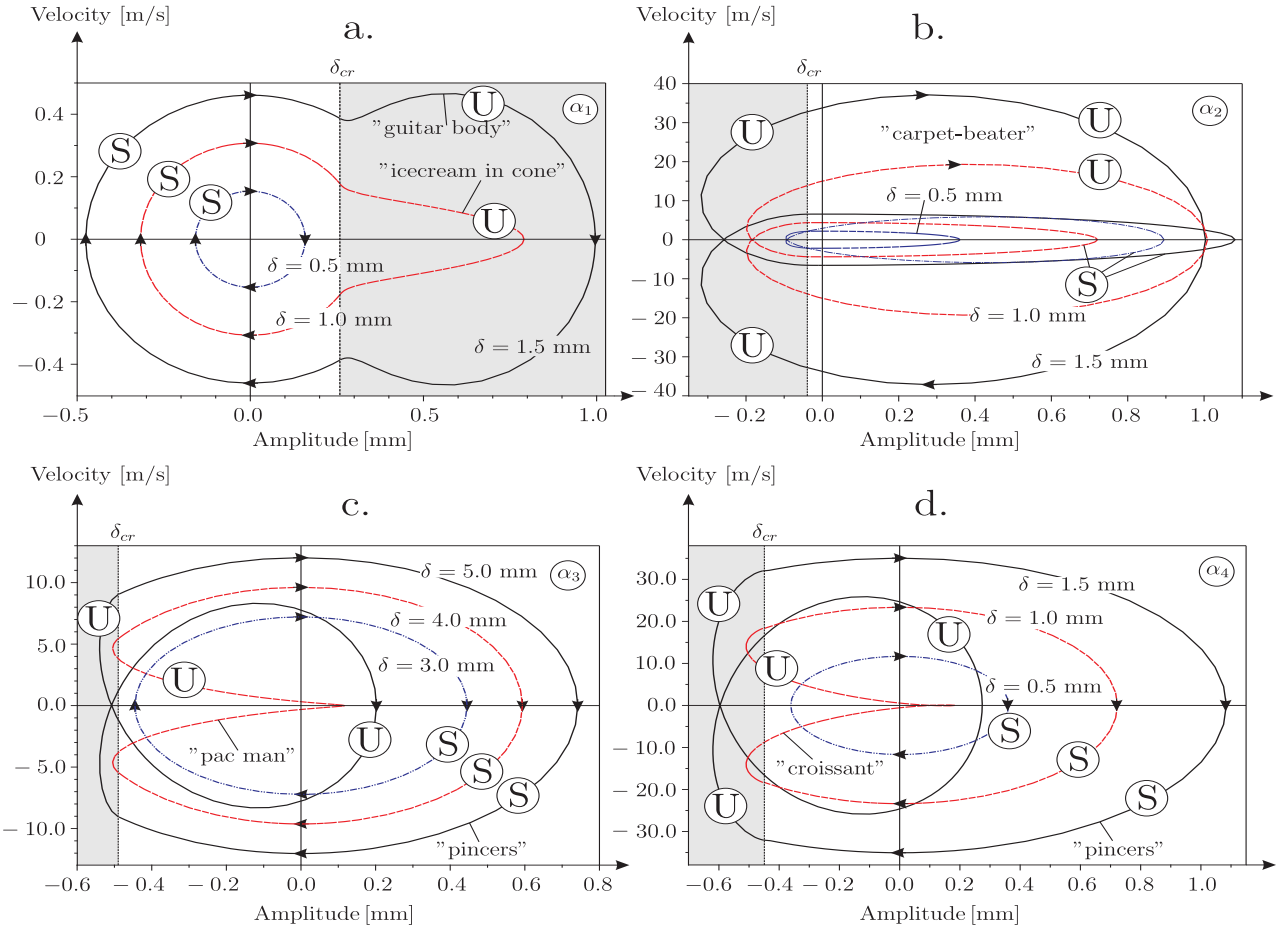

Fig. 18 Phase plane portraits for the midpoint of the delamination (point C in Fig. 1) in the 80/6 beam for the first four free vibration frequencies

VIII. Conclusions

In this paper, the free vibration problem of delaminated composite beams was investigated. The main idea was that the delamination opening during the vibration is induced by the buckling phenomenon and not by the inertia forces. To prove this assumption, a beam FE model was presented. The formulation was based on the system of exact kinematic conditions (SEKC) by cutting the uncracked part in the plane of the delamination and formulating the kinematic continuity conditions between the top and bottom beams. The delaminated portions were modelled by traditional beam elements. The finite element discretization was carried out based on the strain and kinetic energy of the system. A layered beam element was developed to capture the uncracked part and transition elements were constructed to represent the delamination tips as well as the kinematic connection between the uncracked and delaminated portions. The free vibration frequencies and mode shapes were determined in the usual way. The most important aspect is that it was shown that the delaminated portion is subjected to periodic normal forces resulting in time dependent stiffness and the susceptibility to dynamic delamination buckling during the vibration. It was shown that the distribution of normal forces is constant for the first and second free vibration modes, while it is exponential in the case of the third and fourth ones.

The dynamic stability analysis of delaminated beams was carried out by using Bolotin's harmonic balance method. The time signal of delamination buckling was derived in a kinematically consistent way and it was approximated in the form of a Fourier series. The combination of the equation of motion and the time signal resulted in an infinite determinant with matrix elements providing the critical values of the normal forces in the delaminated region under the vibration with the actual frequency. It was found that the stability limit of normal force is constant in the function of thickness ratio, however it decreases suddenly if the thickness ratio is very small. It was shown that in each case there is a critical beam end amplitude defining the bifurcation point of stability. Below the stability limit, harmonic vibration takes place without delamination opening; however, if the excitation of the system induces higher amplitudes than the critical one, then local instability is expected. Strictly speaking, nonlinear analysis is required in the latter case for further conclusions. Nevertheless, if the top beam of the delaminated part is very thin, then its stiffness and mass is negligibly small and a linear

approximation for the mode shapes and phase plane portraits can be applied. Thus, the free vibration mode shapes and the first buckling eigenshapes were superimposed to each other. The phase plane portraits of the midpoint in the top beam of the delamination were plotted and several shapes were discovered, respectively. Maybe, these results contribute to understand better the dynamics of delaminated beams.

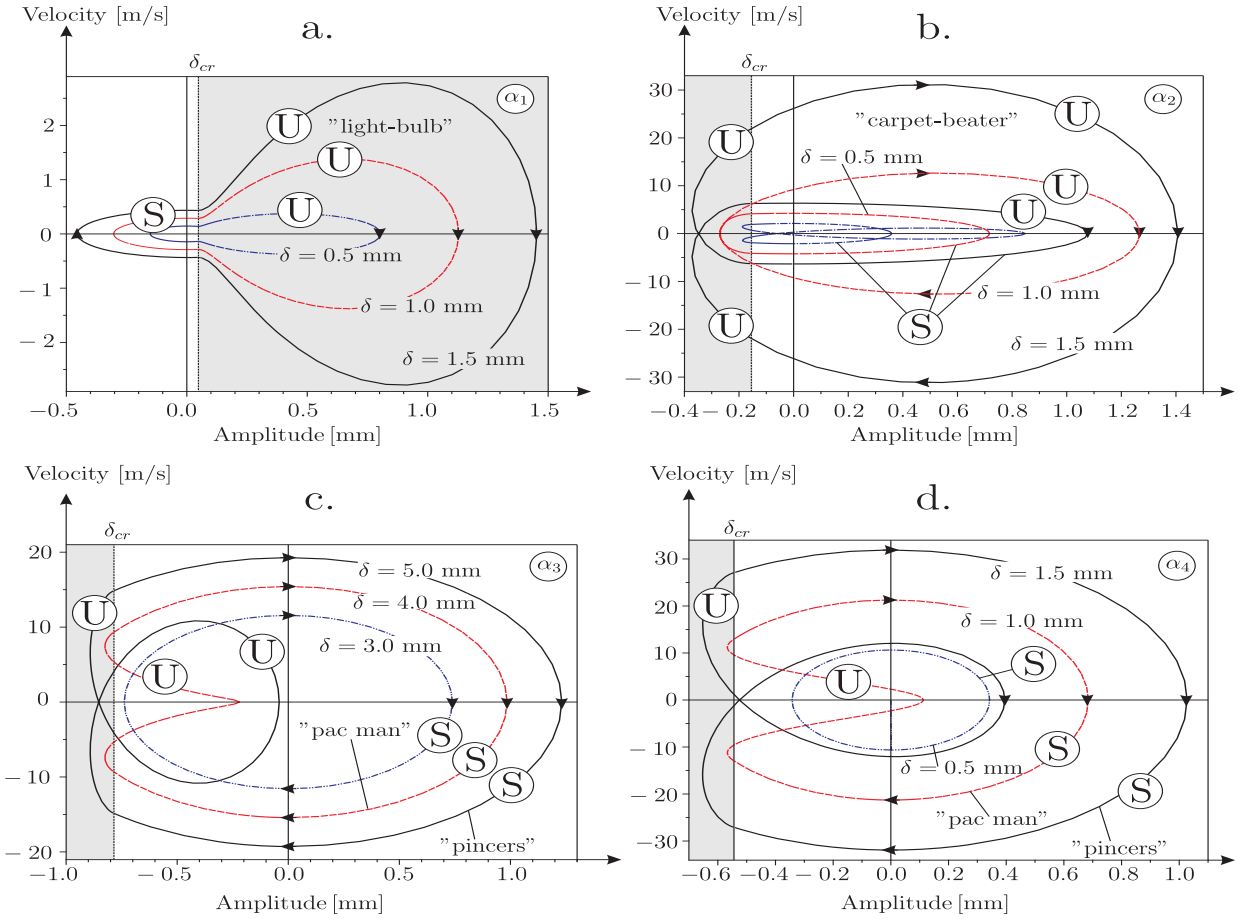

Fig. 19 Phase plane portraits for the midpoint of the delamination (point C in Fig. 1) in the 120/6 beam for the first four free vibration frequencies

Further analysis is required to answer the questions raised by the present analysis. If the thicknesses of the top and bottom layers are close to each other, then the superposition scheme is no longer valid, a nonlinear analysis taking the interaction between global vibration and delamination buckling is necessary.

Acknowledgment

This work was supported by the Hungarian National Scientific Research Fund (OTKA) under grant No.44615-066-15 (108414).

References

[1] J.-F. Zhu, Y. Y Gu, and LTong, "Formulation of reference surface element and its applications in dynamic analysis of delaminated composite beams," *Composite Structures*, vol. 68, no. 4, pp. 481–490, 2005.

[2] B. G. Kiral, "Free vibration analysis of delaminated composite beams," *Science and Engineering of Composite Materials*, vol. 16, no. 3, pp. 209–224, 2009.

[3] N. H. Erdelyi and S. M. Hashemi, "A dynamic stiffness element for free vibration analysis of delaminated layered beams," *Modelling and Simulation in Engineering*, vol. Article ID 492415, 8 pages, 2012.

[4] P. Mujumdar and S. Suryanarayan, "Flexural vibration of beams with delaminations," *Journal of Sound and Vibration*, vol. 125, no. 3, pp. 441–461, 1988.

[5] M.-H. Shen and J. Grady, "Free vibrations of delaminated beams," *AIAA Journal*, vol. 30, no. 5, pp. 1361–1370, 1992.

[6] M. H. Kargarnovin, M. T. Ahmadian, R. A. Jafari-Talookolaei, and M. Abedi, "Semi-analytical solution for the free vibration analysis of generally laminated composite Timoshenko beams with single delamination," *Composites Part B: Engineering*, vol. 45, no. 1, pp. 587-600, 2013.

[7] H. Luo and S. Hanagud, "Dynamics of delaminated beams," *International Journal of Solids and Structures*, vol. 37, pp. 1501–1519, 2000.

[8] S. Lee, T. Park, and G. Z. Voyiadjis, "Vibration analysis of multidelaminated beams," *Composites Part B - Engineering*, vol. 34, pp. 647–659, 2003.

[9] T. Park and a. G. Z. V. S Lee, "Recurrent single delaminated beam model for vibration analysis of multidelaminated beams," *Journal of Engineering Mechanics*, vol. 130, no. 9, pp. 1072–1082, 2004.
[10] R.-A. Jafari-Talookolaei and M. Abedi, "Analytical solution for the freevibration analysis of delaminated Timoshenko beams," *The Scientific World Journal*, 2014, article ID: 280256.
[11] J. Lee, "Free vibration analysis of delaminated composite beams," *Computers and Structures*, vol. 74, pp. 121–129, 2000.
[12] H. Tang, C. Wu, and X. Huang, "Vibration analysis of a coupled beam sdof system by using the recurrence equation method," *Journal of Sound and Vibration*, vol. 311, pp. 912–923, 2008.
[13] N. Hu, H. Fukunaga, M. Kameyama, Y. Aramaki, and F. Chang, "Vibration analysis of delaminated composite beams and plates using a higher-order finite element," *International Journal of Mechanical Sciences*, vol. 44, pp. 1479–1503, 2002.
[14] A. Chakraborty, D. R. Mahapatra, and S. Gopalakrishnan, "Finite element analysis of free vibration and wave propagation in asymmetric composite beams with structural discontinuities," *Composite Structures*, vol. 55, pp. 23–26, 2002.
[15] E. Manoach, J. Warminski, and A. Warminska, "Large amplitude vibrations of heated timoshenko beams with delamination," *Proceedings of the Institution of Mechanical Engineers, Part C: Journal of Mechanical Engineering Science*, vol. 230, no. 1, pp. 88–101, 2016.
[16] A. Szekrényes, "Coupled flexural-longitudinal vibration of delaminated composite beams with local stability analysis," *Journal of sound and vibration*, vol. 333, pp. 5141–5164, 2014.
[17] A. Szekrényes, "The system of exact kinematic conditions and application to delaminated first-order shear deformable composite plates," *International Journal of Mechanical Sciences*, vol. 77, pp. 17–29, 2013.
[18] Z. Szabó, "Nonlinear vibrations of parametrically excited complex mechanical systems," Ph.D. dissertation, Budapest University of Technology and Economics, Department of Applied Mechanics, Budapest, 2001.
[19] Z. Szabó and G. Lóránt, "Parametric excitation of a single railway wheelset," *Vehicle System Dynamics*, vol. 33, no. 1, pp. 49–55, 2000.
[20] D. Bachrathy and G. Stépán, "Efficient stability chart computation for general delayed linear time periodic systems," in *Proceedings of the ASME 2013 International Design Engineering Technical Conferences and Computers and Information in Engineering Conference*, 2013, pp. 1–9, iDETC/CIE 2013, August 4-7, Portland, Oregon, USA, DETC2013-13660.
[21] D. Bachrathy and G. Stépán, "Improved prediction of stability lobes with extended multi frequency solution," *CIRP Annals – Manufacturing Technology*, vol. 62, pp. 411–414, 2013.
[22] Z. Dombóvári, A. Iglesias, M. Zatarain, and T. Insperger, "Prediction of multiple dominant chatter frequencies in milling processes," *International Journal of Machine Tools and Manufacture*, vol. 51, no. 6, pp. 457–464, 2011.
[23] M. Zatarain, J. Alvarez, I. Bediaga, J. Munoa, and Z. Dombóvári, "Implicit subspace iteration as an efficient method to compute milling stability lobe diagrams," *International Journal of Advanced Manufacturing Technology*, vol. 77, no. 1-4, pp. 597–607, 2015.
[24] T. Insperger and G. Stépán, *Semi-discretization of time-delay systems*. New York, Dordrecht, Heidelberg, London: Springer, 2011.
[25] D. Lehotzky, T. Insperger, and G. Stépán, "Extension of the spectral element method for stability analysis of time-periodic delay-differential equations with multiple and distributed delays," *Communications in Nonlinear Science and Numerical Simulation*, vol. 35, pp. 177–189, 2016.
[26] W. W. Bolotin, *Kinetische Stabilit¨at Elastischer Systeme*. VEB Deutscher Verlag der Wissenschaften, Berlin, 1961.
[27] A. Szekrényes, "Bending solution of third-order orthotropic Reddy plates with asymmetric interfacial crack," *International Journal of Solids and Structures*, vol. 51, pp. 2598–2619, 2014.
[28] L. Kollár and G. Springer, *Mechanics of Composite Structures*. Cambridge, New York, Melbourne, Madrid, Capetown, Sao Paolo: Cambridge University Press, 2002.
[29] J. N. Reddy, *Mechanics of laminated composite plates and shells - Theory and analysis*. Boca Raton, London, New York, Washington D.C.: CRC Press, 2004.
[30] M. Petyt, *Introduction to Finite Element Vibration Analysis*, 2nd ed. Cambridge, New York, Melbourne, Madrid, Cape Town, Singapore, São Paulo, Delhi, Dubai, Tokyo, Mexico City: Cambridge University Press, 2010.
[31] K.-J. Bathe, *Finite Element Procedures*. New Jersey 17458: Prentice Hall, Upper Saddle River, 1996.
[32] A. Szekrényes, "A special case of parametrically excited systems: free vibration of delaminated composite beams," *European journal of Mechanics A/Solids*, vol. 49, pp. 82–105, 2015.
[33] N. H. Erdelyi and S. M. Hashemi, "On the finite element free vibration analysis of delaminated layered beams: A new assembly technique," *Shock and Vibration*, vol. Article ID 3707658, 14 pages, 2016.
[34] L. Briseghella, C. Majorma, and C. Pellegrino, "Dynamic stability of elastic structures: a finite element approach," *Computers and Structures*, vol. 69, pp. 11–25, 1998.
[35] A. G. Radu and A. Chattopadhyay, "Dynamic stability analysis of composite plates including delaminations using a higher order theory and transformation matrix approach," *International Journal of Solids and Structures*, vol. 39, pp. 1949–1965, 2002.
[36] A. Chattopadhyay and A. G. Radu, "Dynamic instability of composite laminates using a higher order theory," *Computers and Structures*, vol. 77, pp. 453–460, 2000.
[37] C. M. Saravia, S. P. Machado, and V. H. Cortínez, "Free vibration and dynamic stability of rotating thin-walled composite beams," *European Journal of Mechanics A/Solids*, vol. 30, pp. 432–441, 2011.
[38] F. Pápai, S. Adhikari, and B. Wang, "Estimation of modal dampings for unmeasured modes," *Slovak Journal of Civil Engineering*, vol. XX, no. 4, pp. 17–27, 2012.
[39] G. Catania and S. Sorrentino, "Experimental evaluation of the damping properties of beams and thin-walled structures made of polymeric materials," in *Proceedings of the IMAC-XXVII*. Society of Experimental Mechanics Inc., 2009, pp. 1–10, february 9-12, Orlando, Florida, USA.
[40] J. Peringer, "Dynamics of delaminated composite beams," Master's thesis, Budapest University of Technology and Economics, Department of Applied Mechanics, 2012.
[41] A. Szekrényes, "Natural vibration-induced parametric excitation in delaminated Kirchhoff plates," *Journal of Composite Materials*, 2015, doi:10.1177/0021998315603111.

A. Szekrényes graduated from the Department of Applied Mechanics, Faculty of Mechanical Engineering, Budapest University of Technology and Economics (BUTE), Budapest, Hungary, in 2000. He continued his research in the field of fracture mechanics and mechanics of composite materials within the scope of a national doctoral program at BUTE and obtained his Ph.D. degree in 2006. In 2007 he became an Assistant Professor and in 2011 Associate Professor at the Department of Applied Mechanics. He published 40 papers in international journals and took part in several international conferences. Dr. Szekrényes is available as reviewer in several international journals.